Research Article | Vol. 25, No. 11 | 29 May 2017 | OPTICS EXPRESS 12349

Optics EXPRESS

Terahertz vortex beam generator based on a photopatterned large birefringence liquid crystal

SHIJUN GE,[1] PENG CHEN,[1] ZHIXIONG SHEN,[1] WENFENG SUN,[2] XINKE WANG,[2,3] WEI HU,[1,*] YAN ZHANG,[2] AND YANQING LU[1]

[1]*National Laboratory of Solid State Microstructures, College of Engineering and Applied Sciences, and Collaborative Innovation Center of Advanced Microstructures, Nanjing University, Nanjing 210093, China*

[2]*Department of Physics, Capital Normal University, Beijing Key Laboratory of Metamaterials and Devices, Key Laboratory of Terahertz Optoelectronics, Ministry of Education, and Beijing Advanced Innovation Center for Imaging Technology, Beijing 100048, China*

[3]*wxk82721@cnu.edu.cn*

[*]*huwei@nju.edu.cn*

Abstract: A terahertz (THz) q-plate is proposed and demonstrated to generate THz vortex beams. It is composed of a large birefringence liquid crystal (LC) with spatially-varying director distribution sandwiched by two pieces of fused silica glass. A polarization-sensitive alignment agent is photopatterned to carry out the specific LC director distribution. THz vortex beams with different topological charges are characterized with a THz digital holographic imaging system. The intensity and phase distributions consistent with theoretical analyses are obtained. Besides, an eight-lobed intensity distribution is observed corresponding to the vertical polarization component of a cylindrical vector beam. This work may inspire novel THz applications.

OCIS codes: (160.3710) Liquid crystals; (230.3720) Liquid-crystal devices; (110.6795) Terahertz imaging; (050.4865) Optical vortices.

References and links

1. X. C. Zhang and J. Xu, *Introduction to THz Wave Photonics* (Springer, 2010).
2. S. Koenig, D. Lopez-Diaz, J. Antes, F. Boes, R. Henneberger, A. Leuther, A. Tessmann, R. Schmogrow, D. Hillerkuss, R. Palmer, T. Zwick, C. Koos, W. Freude, O. Ambacher, J. Leuthold, and I. Kallfass, "Wireless sub-THz communication system with high data rate," Nat. Photonics **7**(12), 977–981 (2013).
3. L. Allen, M. W. Beijersbergen, R. J. Spreeuw, and J. P. Woerdman, "Orbital angular momentum of light and the transformation of Laguerre-Gaussian laser modes," Phys. Rev. A **45**(11), 8185–8189 (1992).
4. J. Wang, J. Y. Yang, I. M. Fazal, N. Ahmed, Y. Yan, H. Huang, Y. Ren, Y. Yue, S. Dolinar, M. Tur, and A. E. Willner, "Terabit free-space data transmission employing orbital angular momentum multiplexing," Nat. Photonics **6**(7), 488–496 (2012).
5. F. Tamburini, E. Mari, A. Sponselli, B. Thidé, A. Bianchini, and F. Romanato, "Encoding many channels on the same frequency through radio vorticity: first experimental test," New J. Phys. **14**(3), 033001 (2012).
6. T. Lei, M. Zhang, Y. R. Li, P. Jia, G. N. Liu, X. G. Xu, Z. H. Li, C. J. Min, J. Lin, C. Y. Yu, H. B. Niu, and X. C. Yuan, "Massive individual orbital angular momentum channels for multiplexing enabled by dammann gratings," Light Sci. Appl. **4**(3), e257 (2015).
7. E. A. Nanni, W. R. Huang, K.-H. Hong, K. Ravi, A. Fallahi, G. Moriena, R. J. Miller, and F. X. Kärtner, "Terahertz-driven linear electron acceleration," Nat. Commun. **6**, 8486 (2015).
8. K. Miyamoto, K. Suizu, T. Akiba, and T. Omatsu, "Direct observation of the topological charge of a terahertz vortex beam generated by a Tsurupica spiral phase plate," Appl. Phys. Lett. **104**(26), 261104 (2014).
9. X. Wang, J. Shi, W. Sun, S. Feng, P. Han, J. Ye, and Y. Zhang, "Longitudinal field characterization of converging terahertz vortices with linear and circular polarizations," Opt. Express **24**(7), 7178–7190 (2016).
10. B. A. Knyazev, Y. Y. Choporova, M. S. Mitkov, V. S. Pavelyev, and B. O. Volodkin, "Generation of terahertz surface plasmon polaritons using nondiffractive Bessel beams with orbital angular momentum," Phys. Rev. Lett. **115**(16), 163901 (2015).
11. Z. Xie, X. Wang, J. Ye, S. Feng, W. Sun, T. Akalin, and Y. Zhang, "Spatial terahertz modulator," Sci. Rep. **3**(1), 3347 (2013).

#291781 https://doi.org/10.1364/OE.25.012349
Journal © 2017 Received 30 Mar 2017; revised 10 May 2017; accepted 10 May 2017; published 17 May 2017

Optics EXPRESS

12. J. He, X. Wang, D. Hu, J. Ye, S. Feng, Q. Kan, and Y. Zhang, "Generation and evolution of the terahertz vortex beam," Opt. Express **21**(17), 20230–20239 (2013).
13. R. Imai, N. Kanda, T. Higuchi, K. Konishi, and M. Kuwata-Gonokami, "Generation of broadband terahertz vortex beams," Opt. Lett. **39**(13), 3714–3717 (2014).
14. A. Minasyan, C. Trovato, J. Degert, E. Freysz, E. Brasselet, and E. Abraham, "Geometric phase shaping of terahertz vortex beams," Opt. Lett. **42**(1), 41–44 (2017).
15. C. J. Lin, Y. T. Li, C. F. Hsieh, R. P. Pan, and C. L. Pan, "Manipulating terahertz wave by a magnetically tunable liquid crystal phase grating," Opt. Express **16**(5), 2995–3001 (2008).
16. I. C. Ho, C. L. Pan, C. F. Hsieh, and R. P. Pan, "Liquid-crystal-based terahertz tunable Solc filter," Opt. Lett. **33**(13), 1401–1403 (2008).
17. X. W. Lin, J. B. Wu, W. Hu, Z. G. Zheng, Z. J. Wu, G. Zhu, F. Xu, B. B. Jin, and Y. Q. Lu, "Self-polarizing terahertz liquid crystal phase shifter," AIP Adv. **1**(3), 032133 (2011).
18. S. J. Ge, J. C. Liu, P. Chen, W. Hu, and Y. Q. Lu, "Tunable terahertz filter based on alternative liquid crystal layers and metallic slats," Chin. Opt. Lett. **13**(12), 120401 (2015).
19. L. Wang, X. W. Lin, W. Hu, G. H. Shao, P. Chen, L. J. Liang, B. B. Jin, P. H. Wu, H. Qian, Y. N. Lu, X. Liang, Z. G. Zheng, and Y. Q. Lu, "Broadband tunable liquid crystal terahertz waveplates driven with porous graphene electrodes," Light Sci. Appl. **4**(2), e253 (2015).
20. L. Marrucci, C. Manzo, and D. Paparo, "Optical spin-to-orbital angular momentum conversion in inhomogeneous anisotropic media," Phys. Rev. Lett. **96**(16), 163905 (2006).
21. S. Slussarenko, A. Murauski, T. Du, V. Chigrinov, L. Marrucci, and E. Santamato, "Tunable liquid crystal q-plates with arbitrary topological charge," Opt. Express **19**(5), 4085–4090 (2011).
22. E. Karimi, B. Piccirillo, E. Nagali, L. Marrucci, and E. Santamato, "Efficient generation and sorting of orbital angular momentum eigenmodes of light by thermally tuned q-plates," Appl. Phys. Lett. **94**(23), 231124 (2009).
23. L. Marrucci, E. Karimi, S. Slussarenko, B. Piccirillo, E. Santamato, E. Nagali, and F. Sciarrino, "Spin-to-orbital conversion of the angular momentum of light and its classical and quantum applications," J. Opt. **13**(6), 064001 (2011).
24. W. Ji, C. H. Lee, P. Chen, W. Hu, Y. Ming, L. Zhang, T. H. Lin, V. Chigrinov, and Y. Q. Lu, "Meta-q-plate for complex beam shaping," Sci. Rep. **6**(1), 25528 (2016).
25. V. G. Chigrinov, V. M. Kozenkov, and H. S. Kwok, *Photoalignment of Liquid Crystalline Materials: Physics and Applications* (John Wiley and Sons, 2008).
26. H. Wu, W. Hu, H. C. Hu, X. W. Lin, G. Zhu, J. W. Choi, V. Chigrinov, and Y. Q. Lu, "Arbitrary photo-patterning in liquid crystal alignments using DMD based lithography system," Opt. Express **20**(15), 16684–16689 (2012).
27. V. Chigrinov, S. Pikin, A. Verevochnikov, V. Kozenkov, M. Khazimullin, J. Ho, D. D. Huang, and H. S. Kwok, "Diffusion model of photoaligning in azo-dye layers," Phys. Rev. E Stat. Nonlin. Soft Matter Phys. **69**(6 Pt 1), 061713 (2004).
28. L. Wang, X. W. Lin, X. Liang, J. B. Wu, W. Hu, Z. G. Zheng, B. B. Jin, Y. Q. Qin, and Y. Q. Lu, "Large birefringence liquid crystal material in terahertz range," Opt. Mater. Express **2**(10), 1314–1319 (2012).
29. P. Chen, B. Y. Wei, W. Ji, S. J. Ge, W. Hu, F. Xu, V. Chigrinov, and Y. Q. Lu, "Arbitrary and reconfigurable optical vortex generation: a high-efficiency technique using director-varying liquid crystal fork gratings," Photonics Res. **3**(4), 133–139 (2015).
30. B. Wang, B. Quan, J. He, Z. Xie, X. Wang, J. Li, Q. Kan, and Y. Zhang, "Wavelength de-multiplexing metasurface hologram," Sci. Rep. **6**(1), 35657 (2016).
31. Z. Jiang, X. G. Xu, and X. C. Zhang, "Improvement of terahertz imaging with a dynamic subtraction technique," Appl. Opt. **39**(17), 2982–2987 (2000).
32. X. Wang, Y. Cui, W. Sun, J. Ye, and Y. Zhang, "Terahertz polarization real-time imaging based on balanced electro-optic detection," J. Opt. Soc. Am. A **27**(11), 2387–2393 (2010).
33. Q. Zhan, "Cylindrical vector beams: from mathematical concepts to applications," Adv. Opt. Photonics **1**(1), 1–57 (2009).
34. P. Chen, W. Ji, B. Y. Wei, W. Hu, V. Chigrinov, and Y. Q. Lu, "Generation of arbitrary vector beams with liquid crystal polarization converters and vector-photoaligned q-plates," Appl. Phys. Lett. **107**(24), 241102 (2015).
35. B. Y. Wei, W. Hu, Y. Ming, F. Xu, S. Rubin, J. G. Wang, V. Chigrinov, and Y. Q. Lu, "Generating switchable and reconfigurable optical vortices via photopatterning of liquid crystals," Adv. Mater. **26**(10), 1590–1595 (2014).

1. Introduction

Terahertz (THz) waves, typically 0.1~10 THz in electromagnetic spectrum, hold great potentials in high-speed wireless communication [1, 2]. Mode-division multiplexing technology can drastically enhance the capacity of optical communication systems. Specifically, orbital angular momentum (OAM) [3] adds a new degree of freedom in the manipulation of light, thus providing infinite number of eigenstates. It is carried by the optical vortex beam featured with a spiral wavefront, and quantized as $m\hbar$ per photon where m is the topological charge. OAM-based (de-)multiplexing has exhibited its superiority in both optical

Optics EXPRESS

and wireless communications [4–6]. Similar strategy can be extended to THz range as well, making THz vortex beams attractive. In addition to high-speed wireless communication, THz vortex beams are also promising in electron acceleration [7], high-spatial-resolution THz imaging and even some uncharted territories.

Several methods have been developed to generate THz vortex beams. Spiral phase plates can directly rephase THz Gaussian beams into THz vortex beams [8,9]. Computer-generated holograms (CGHs) imprinted in silicon [10] and formed by photo-generated carrier pattern [11] are also employed. Metasurfaces consisting of V-shape antennas can modulate the local phase to generate THz vortex beams [12]. Recently, segmented half-wave plates with specially designed optical axes are implemented [13, 14]. However, these elements are either lack of tunability and switchability, or suffer from low efficiency, which are key requirements to handle THz waves. Thanks to the external field responsiveness, liquid crystal (LC) has proven to be a very promising candidate for tunable THz devices [15–18]. A broadband electrically tunable LC THz wave plate is realized [19], supplying a practical way for THz beam tailoring.

In this work, we propose and demonstrate a THz q-plate by introducing a large birefringence LC to generate THz vortex beams. The spatially-varying LC orientation is accomplished by a dynamic micro-lithography based photopatterning technique. The intensity and phase distributions of THz vortex beams with different topological charges are characterized. This work may pave a road towards THz vortex beam generation and prompt applications in THz imaging, communication, *etc*.

2. Principle

Q-plate [20, 21], one of geometric phase optical elements, plays a crucial role in classical and quantum optics, due to the coupling between spin angular momentum (SAM) and OAM [22–24]. The q-plate is essentially an inhomogeneous wave plate, whose optical axes are homogeneous along z-axis and the orientation angle α with respect to x-axis in the x-y plane obey the following equation [20]:

$$\alpha = q\varphi + \alpha_0, \tag{1}$$

where $\varphi = \arctan(y/x)$ is the azimuthal angle, q is the topological charge of the q-plate, and α_0 is the initial angle when $\varphi = 0$ and is usually assumed to be zero since it does not affect the resultant OAM. According to Eq. (1), the optical axis distribution of a q-plate with $q = 0.5$ is calculated and shown as inset (a) in Fig. 1. The color variation from blue to red indicates the optical axis orientation varying from 0° to 180° continuously.

The photonic spin-orbital interaction in a q-plate can be analyzed through Jones matrix calculation. The Jones matrix for the q-plate is:

$$\begin{aligned} \mathbf{J} &= \mathbf{R}(-\alpha)\cdot\begin{bmatrix} \exp(-i\Gamma/2) & 0 \\ 0 & \exp(i\Gamma/2) \end{bmatrix}\cdot\mathbf{R}(\alpha), \\ &= \cos\zeta\,\mathbf{I} - i\sin\zeta\begin{bmatrix} \cos 2\alpha & \sin 2\alpha \\ \sin 2\alpha & -\cos 2\alpha \end{bmatrix} \end{aligned} \tag{2}$$

where $\mathbf{I}$ is the identity matrix, $\zeta = \pi\Delta n d/\lambda$ is the half of the phase retardation Γ, Δn is the birefringence, d is the thickness and λ is the wavelength of the incident wave. Consider a circularly polarized beam, it can be described as $\mathbf{E}_{\text{in}} = \chi^{(\pm)} = 1/\sqrt{2}\begin{pmatrix}1 & \pm i\end{pmatrix}^{\text{T}}$, the two spin eigenstates corresponding to left (+) and right (–) circular polarization states, respectively. After passing through the q-plate, the output wave can be expressed as:

Optics EXPRESS

$$\begin{aligned}\mathbf{E}_{out} &= \mathbf{J}\cdot\mathbf{E}_{\text{in}} \\ &= \cos\zeta\cdot\chi^{(\pm)} - i\sin\zeta\cdot\exp[\pm i2q\varphi]\cdot\chi^{(\mp)}.\end{aligned} \tag{3}$$

In the case of a left circularly polarized incident wave, the emerging wave is a superposition of two parts: the residual left circularly polarized component without change, and the transformed right circularly polarized one with a spiral phase factor $\exp(i2q\varphi)$, corresponding to a vortex beam with $m = 2q$. Vice versa, for right circular incident polarization, the transformed left circularly polarized one has a sign-inverted orbital helicity. Additionally, the intensity distribution between the residual and the transformed component depends on the phase retardation of the q-plate. According to Eq. (3), the conversion efficiency, defined as the intensity ratio of the transformed vortex components to the total transmit wave, is $\sin^2(\zeta)$. For the special case of half-wave condition ($\Gamma = \pi$), the residual component is wholly suppressed and the output is a pure vortex beam. In other cases, the transformed component (vortex beam) can be extracted out by a quarter-wave plate and a polarizer.

3. Photopatterning technique

Owing to the pronounced optical birefringence and controllable director (*i.e.*, local optical axis) distribution, LC becomes the first choice for q-plate fabrication. To realize a LC THz q-plate, a dynamic photopatterning technique which is quite suitable for high-resolution multi-domain alignment of LC is employed [25, 26]. Here, sulphonic azo-dye SD1 (Dai-Nippon Ink and Chemicals, Japan) is used as the photoalignment agent, which is polarization-sensitive and intends to lie perpendicularly to illuminated UV polarization [27]. To get enough phase retardation for the large-wavelength THz wave, we adopt a home-made LC NJU-LDn-4 with an average birefringence of 0.306 in the range of 0.5 to 2.5 THz [28]. And a 250 μm cell gap is chosen to obtain maximum phase retardation (0.5π at 1.0 THz) while guaranteeing good alignment effect.

Fused silica glass substrates are oxygen-plasma cleaned and then spin-coated with a 0.5% solution of SD1 in dimethylformamide. Two SD1-coated substrates are assembled together and sealed with epoxy glue to form an empty cell separated by 250 μm-thick Mylar films. Then, a digital micro-mirror device based dynamic micro-lithography setup is applied to perform a multi-step partly-overlapping exposure (see details in [29]). The quasi-continuously spatially-varying orientation of SD1 is carried out. After the LC NJU-LDn-4 is infiltrated, a continuously spatially-varying LC orientation corresponding to the designed q-plate is obtained. The photo of a q-plate with $q = 0.5$ under crossed polarizers are shown in the inset (b) in Fig. 1. Twice ($4q$) bright-to-dark alternations is observed. The change of brightness corresponds to the variation of angles between the LC director and the polarizer.

Optics EXPRESS

4. Generation and characterization of THz vortex beams

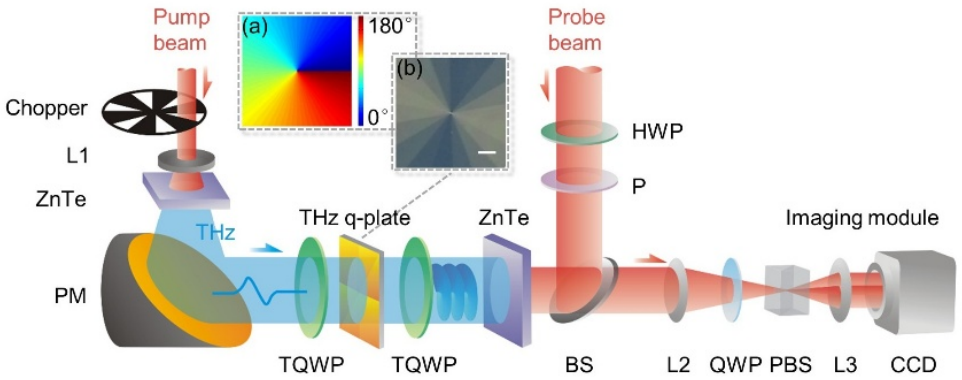

Fig. 1. THz digital holographic imaging system. Insets: (a) the theoretical optical axis distribution and (b) photo under crossed polarizers of a q-plate with q = 0.5. The scale bar is 1 mm.

To characterize the field distribution of generated THz vortex beams, a THz digital holographic imaging system is utilized [30]. As shown in Fig. 1, the light source is a Spectra-Physics femtosecond laser amplifier (central wavelength: 800 nm, pulse duration: 50 fs, average power: 900 mW, and repetition ratio: 1 kHz). The laser pulse is split into pump and probe beams for exciting and detecting THz radiations, respectively. The pump beam with an 890 mW average power is expanded by a concave lens (L1) with a 25 mm focal length (f). A 3 mm-thick <110> ZnTe crystal is mounted close to L1 and illuminated by the pump beam. Due to the optical rectification effect, a linearly polarized THz beam is excited. A parabolic mirror (PM, f = 75 mm) is used to collimate the THz beam. A 1.0 THz quarter-wave plate (TQWP) is inserted after the PM to prepare a circularly polarized THz incident beam. The THz beam with 8 mm diameter subsequently emerges through the LC THz q-plate. The other TQWP following the q-plate changes the generated THz field components with orthogonal circular polarizations into two linearly polarized ones (horizontal and vertical) respectively. Another ZnTe crystal is used to detect the transmitted linearly polarized wave. The distance between TQWP and detecting crystal is 5 millimeters.

To measure different THz polarization components, a half wave plate (HWP) and a polarizer (P) are adopted to adjust the polarization of probe beam, which is then reflected onto the detecting crystal by a 50/50 non-polarization beam splitter (BS). Due to the linear electro-optic effect in the detection crystal induced by the THz field, the probe polarization is modulated to carry corresponding THz information. The reflected probe beam is sent into the imaging module of the system to measure the probe-polarization variation, which consists of a QWP, a Wollaston prism (PBS), two lenses (L2 and L3), and a CCD camera (frame rate: 4 Hz). The inserted mechanical chopper is synchronously controlled with the CCD camera. The two-dimensional THz information can be extracted by using the dynamic subtraction and balanced electro-optic detection techniques [31, 32]. In this system, the size of the imaging region is 8 mm × 8 mm. By varying the optical path difference between the THz and probe beams continuously, a series of THz images in the time domain are recorded. 100 frames are averaged at each scan point to enhance the signal-to-noise ratio. The intensity and phase information of each spectral component are extracted through operating the Fourier transformation to THz temporal images.

Optics EXPRESS

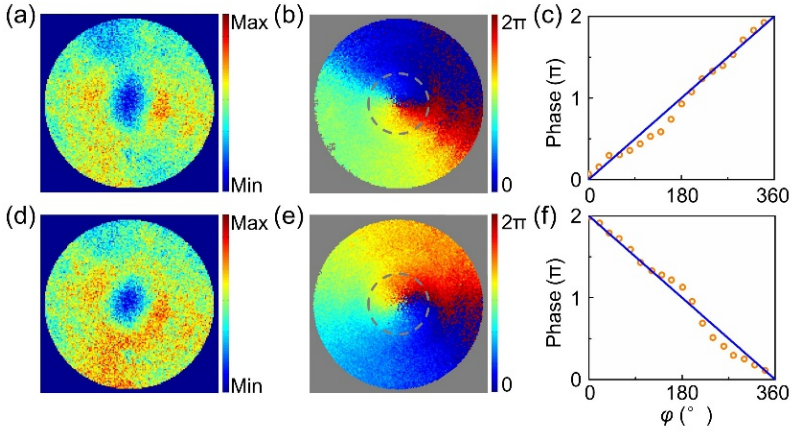

Fig. 2. The measured intensity and phase distribution of the transformed component of the q-plate with q = 0.5 at 1.0 THz, when incident polarization is (a) and (b) left, (d) and (e) right circular polarization. (c) and (f) the phase dependence of the azimuthal angle along the circle line marked in (b) and (e), respectively, where markers indicate experimental data and solid lines are theoretical calculations.

Via switching the polarization of the probe beam, we can detect two orthogonal linearly polarized components of the output THz beam corresponding to its orthogonal circularly polarized components, respectively. A LC THz q-plate with q = 0.5 is characterized at 1.0 THz as an example. When the incident is left circular polarization, the intensity and phase distributions of the transformed component are shown in Figs. 2(a) and 2(b). The intensity profile is donut-like owing to the phase singularity at the beam center. The dependence of the phase on the azimuthal angle is quantitatively exhibited in Fig. 2(c), and it is in good agreement with the theoretical linear relation $\Phi=\varphi$ of a spiral phase. It reveals that the right circularly polarized component is a THz vortex beam with m = + 1. On the other hand, for right circularly polarized THz beam, the transformed component forms a vortex beam with m = –1, which is presented in Figs. 2(d)-2(f).

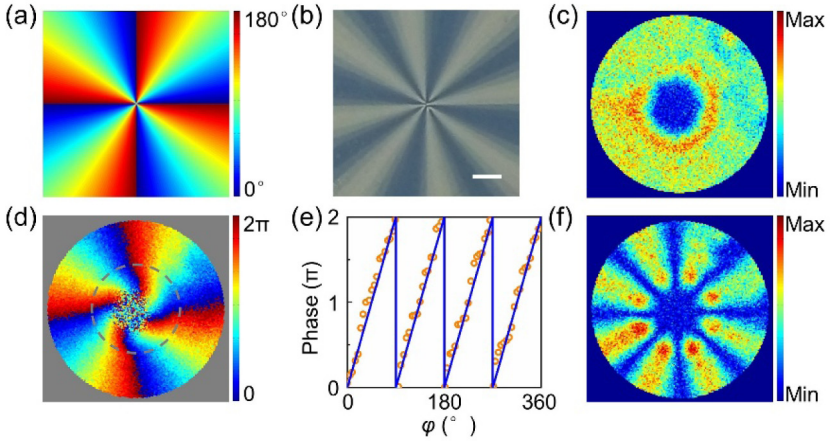

Fig. 3. (a) The theoretical optical axis distribution and (b) the photo under crossed polarizers of the q-plate with q = 2, the scale bar is 1 mm. (c) The measured intensity and (d) phase distributions of the transformed component at 1.0 THz with left circular incident polarization. (e) The phase dependence of the azimuthal angle along the circle line marked in (d), where markers indicate experimental data and solid line is theoretical calculation. (f) The vertical polarization component of the output THz beam with horizontal incident THz polarization.

Optics EXPRESS

To further verify the capability of THz vortex beam generation, a LC q-plate with $q = 2$ is fabricated as well. The theoretical optical axis distribution and corresponding photo under crossed polarizers are shown in Figs. 3(a) and 3(b), respectively. Eight times bright-to-dark alternations exist as expectation. Figures 3(c) and 3(d) exhibit the intensity and phase distributions of the transformed right circular polarization component for a left circularly polarized incident beam. The central dark region becomes larger due to the larger m value. There are four times 0 to 2π linear phase gradience as depicted in Fig. 3(e), consistent with a THz vortex beam of $m = +4$.

In addition, when the incident polarization is linear polarization, which could be regarded as a superposition of two orthogonal circular polarizations, the output THz beam is thus a superposition of four parts: the residual left and right circularly polarized components, the transformed right and left circular polarization with a phase factor $\exp(i4\varphi)$ and $\exp(-i4\varphi)$, respectively. On the other hand, the former two components have equal intensity, and their superposition forms a linearly polarized part with the same polarization as the incident; while the latter equal-intensity two superpose as a vectorially polarized part, *i.e.*, cylindrical vector beam [33, 34]. To verify it, we detect the vertical polarization component of the output THz beam for horizontal incident polarization. An intensity distribution with eight lobes is obtained as shown in Fig. 3(f), consistent with that of the vertically polarized component of a pure cylindrical vector beam with a polarization order 4.

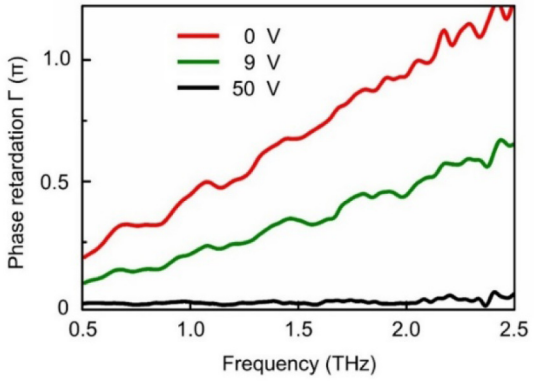

Fig. 4. Frequency dependent phase retardation at different operating voltages.

To demonstrate its electro-optical tunability, few-layer porous graphene films [19] are used as high transparent electrodes to drive the LC. The frequency dependent phase retardations at different operating voltages are exhibited in Fig. 4. Obviously, it can be tuned to satisfy the half-wave condition at any frequency above 2 THz, making the LC THz q-plate suitable for generating pure THz vortex beams in a broad range. The dynamical switch between *on* and *off* states can also be realized by alternating the applied voltage between half-wave voltage and high voltage (50 V as shown in Fig. 4). Owing to the restricted frequency range of the THz system, only results around 1.0 THz are extracted in our experiments. Since the phase retardation is ~0.5π for 1.0 THz, the conversion efficiency of the generated THz vortex beams is ~50%. While the phase change is not so smooth due to the small number of exposure steps, the efficiency of the desired vortex would be slightly lower than 50%. Through stacking cells [19] and increasing the resolution of the exposure process, the conversion efficiency of designed vortex beam can be significantly improved. Moreover, thanks to the optical rewritability of the alignment agent SD1, the LC patterns could be reconfigured [35], making the arbitrary and instant manipulation of THz OAM states possible.

Optics EXPRESS

5. Conclusion

In conclusion, we propose a large birefringence LC THz q-plate. THz vortex beams with different topological charges are demonstrated and corresponding phase and intensity distributions are characterized. Their electrical tunability and switchability are verified. The proposed LC THz q-plate could also be utilized to generate THz cylindrical vector beams. This work supplies an easy and efficient approach for THz vortex generation and has potentials in various applications, such as THz communication, sensing and imaging.

Funding

National Natural Science Foundation of China (NSFC) (Nos. 61490714, 61435008, 61575093, and 11474206).